PHILOSOPHICAL MAGAZINE A, 1999, VOL. 79, NO. 10, 2437–2459

The thick yield surface: idea and approach for investigating its structure

Y. E. BEYGELZIMER† and A. V. SPUSKANYUK‡

Donetsk Physical and Technical Institute of the National Academy of Sciences of Ukraine, 72 R. Luxembourg Street, Donetsk 340114, Ukraine

[*Received 30 June 1998 and accepted in revised form 18 November 1998*]

ABSTRACT

The hypothesis presented in the present work is that the yield surface can be presented as a thick 'foamed surface' with dimensionality exceeding two, that is the yield surface is of a fractal nature. A micromechanical model of a polycrystal based on cellular automata (the cellular model) is proposed to investigate the yield surface structure. A polycrystal representative volume is modelled as a population of interconnected units which, in turn, can consist of lower-scale-level units. Simple units, which do not have an internal structure, are deformed by sliding along the various allowed sliding systems. To consider the stress distribution within the limits of the components, the approach of a self-consistent field is used. The rotation of units and moment stresses connected with it are taken into account. The results of computer experiments show that the number of known plastic deformation effects can be adequately described by the proposed cellular model. The 'thick yield surface' concept allows the additional correlation between micromechanical models of polycrystals and phenomenological theory of plasticity to be determined.

§ 1. INTRODUCTION

Classical plastic flow models do not satisfy modern requirements. There are two main directions in their development. The first, which is mathematical, is connected with the development of the general theory of rheological relationships; the second, which is physical, is connected with the development of the representative volume element (RVE) models which are based on specific ideas about deformation mechanisms. Within the framework of the first approach, the macroscopic experimental data are formalized; the second approach deals the generalization of physical research results for the different scale levels that are involved in plastic deformation.

These approaches have advantages and disadvantages. In phenomenological theories, the advantages are the mathematical simplicity and concise formulation of the constitutive relations, which allows them to be used in practical calculations. However, the mathematical models of this class cannot be considered as general; they are useful only for the description of a limited range of deforming processes. On the other hand, physical theories that are based on the description of real plastic deformation mechanisms are very explanatory and predictive, but they lack mathematical simplicity.

† Email: beigel@hpress.dipt.donetsk.ua
‡ Email: alex@hpress.dipt.donetsk.ua

Philosophical Magazine A ISSN 0141–8610 print/ISSN 1460-6992 online
http://www.tandf.co.uk/JNLS/phm.htm
http://www.taylorandfrancis.com/JNLS/phm.htm

The above circumstances mean that it is necessary to compromise in determining the constitutive relations for the RVE, the structure and parameters of which contain information about the microlevel and mesolevel phenomena. The fundamental work on this has been carried out, for example, by Hill (1972) and Rice (1971).

In the present work we extend the definition of this typically 'macroscopic' concept of a yield surface by including additional information about the material structure in it. The terms a 'thick yield surface' and a 'cloud of internal stresses' are introduced here to fulfil this need.

The yield surface is one of the fundamental concepts of the mathematical theory of plasticity (Hill 1950). It represents a geometric image of the yield condition in the stress space. If a point mapping the stressed condition of the material in this space resides inside the area limited by the yield surface, the material is deformed as elastic. In the case when the indicated point hits on a surface, plastic flow starts. The state mapped by points lying outside the area limited by the yield surface is impossible. There are various interpretations concerning the form of the yield surface and its evolution during the plastic deformations of material. In the study by Koiter (1953) the explanation of sliding theory (Batdorf and Budiansky 1949) is given within the framework of the yield surface approach.

In several investigations the yield surface is represented as a classical surface, that is a two-dimensional object. The hypothesis put forward in the present work is that the yield surface can be presented as a thick 'foamed surface' with dimensionality exceeding two. In other words, perhaps, the yield surface is of a fractal nature, that is it belongs to the class of geometric objects with fractional dimensionality. The properties of such objects have been extensively studied (Mandelbrot 1983). Apparently, the fractal structure of the yield surface is determined by the fractal structure of natural materials.

The RVE of homogeneous materials, inhomogeneous materials and materials with self-similar fractal structure are shown schematically in figure 1.

In many cases, the self-similarity of objects, or 'scaling' as it is called by physicists, has already allowed their structure during the macroscopic description to be taken into account (for example Barrenblatt (1979), De Gennes (1979) and Mandelbrot (1983)), which inspires new attempts to be made to study this, as there is evidence (for example Hornbogen (1986)) on the fractal structure of metal alloys.

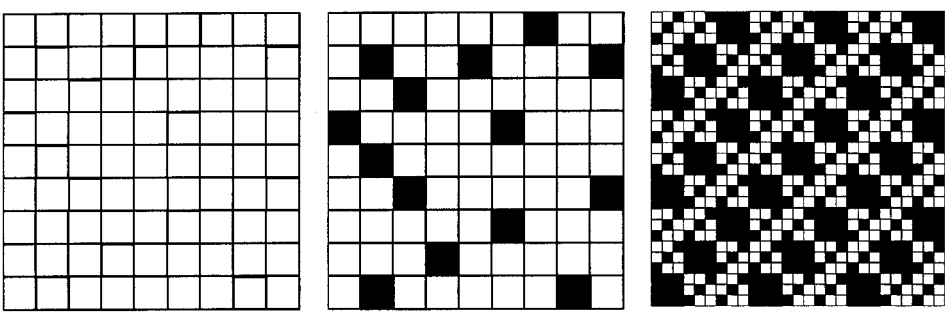

Figure 1. RVE for (*a*) homogeneous materials, (*b*) inhomogeneous materials and (*c*) materials with a self-similar fractal structure.

The idea of how to build a 'thick yield surface' is as follows. The RVE of material is divided into elementary objects (units); each of these is deformed by means of certain mechanisms (in the following these are the so-called simple units that are deformed by dislocation sliding). In the space of stresses the yield surfaces of the indicated objects are drawn as if they were absolutely independent and not connected with each other. The aggregation of all these surfaces forms a 'thick yield surface'. At the same time, to each surface is attributed a certain 'weight', which is proportional to the volume of the appropriate object. Imagine a geometric image obtained after cutting a 'thick yield surface' by an octahedral or other coordinate plane (as is usually done in the mathematical theory of plasticity); it will be a network consisting of many lines. The thickness of each line corresponds to the 'weight' of the appropriate object. In addition, for example, if the sizes of the objects are distributed similarly to the sizes of black cells in figure 1(*c*), we can expect the network obtained to be fractal. These heuristic reasons allow us to assume that the 'thick yield surface' is of a fractal nature.

The interaction of objects, which create the material RVE as a whole, is taken into account through the internal stresses originating between objects during their joint plastic deformation and controlling strain mechanisms acting in them. Points mapping the stressed condition of objects form a 'cloud of internal stresses', the centre of which is the point mapping the stressed condition of the whole RVE.

The interaction of the 'cloud of internal stresses' with the 'thick yield surface' determines the plastic deformation. A more detailed description of this effect is given in § 7.

In accordance with the ideas mentioned above, the construction of the 'thick yield surface' and investigation of the correlation of its parameters with the plastic deformation are reduced to the solution of single problem, that is the strain of the aggregate of interconnected units. Together these units form the material RVE.

A number of methods to solve such problems have been suggested. Among these, we would highlight the two methods that appear to be the most effective: the finite element method (FEM) and the self-consistent scheme. The FEM is used in the mechanics of composites (for example Shen *et al.* (1994)). This method allows the detailed investigation of the stress–strained state of the material RVE. Application of the FEM to study the stressed–strained state of the polycrystalline aggregate, from our point of view, is premature. Firstly, there are not yet sufficiently detailed data about the construction of such an aggregate and the properties of its component elements (e.g. grain boundaries). Secondly, because of the stochastic structure of this aggregate, the in-depth study of just one of several realizations, which is given by the FEM, is too explicit, since averaging on realizations is necessary anyway. In addition, the FEM requires significant resources.

The facts mentioned above lead us to consider now the second of the above-mentioned approaches; the self-consistent scheme. Its essence is that during research on the grain strain within a polycrystalline aggregate it is supposed that this grain is placed in a certain continuum environment where it is surrounded by other grains.

Fundamental studies in this direction have been by Kröner (1961), Budiansky and Wu (1962), Hutchinson (1964) and Hill (1965). Hill (1965) showed that Kröner (1961) implicitly assumed the environment to have purely elastic properties and did not take into account some effects connected with the transition of the aggregate to the plastic state. In particular, Berveiller and Zaoui (1979) showed that the Kröner interaction law does not take into account the plastic accommodation of grains,

which results in an abnormally high estimation of the magnitude of the internal stresses. Hill (1965) proposed a general method in which the law of interaction between a single grain and the environment was not given *a priori* but rather was determined through calculations. This approach allows effects connected with the plastic accommodation of grains to be taken into account. However, because of the absence of experimental methods to determine the required parameters, it did not find a practical application. Berveiller and Zaoui (1979) proposed the original method to consider the elastic–plastic accommodation of grains that was based on the introduction of a simple scalar 'accommodation function'. These workers proposed an effective technique for its determination through the mechanical testing of polycrystals.

In the present work we propose a mathematical model of a polycrystalline aggregate (the cellular model) based on the self-consistent scheme and the law of interaction similar to the law introduced by Berveiller and Zaoui (1979). There are several differences from the classical self-consistent scheme which allow the following:

(*a*) use of the cellular model to study aggregates having an inhomogeneous and fractal structure;
(*b*) consideration of the local character of the grains' interaction (short-range interaction);
(*c*) introduction of various material hardening laws, which are not only linear as in the work of Berveiller and Zaoui (1979).

These differences are possible owing to the use of the cellular automata approach (for example Toffoli and Margolus (1987) and Preston and Duff (1994)). The main ideas of this approach are the following.

(1) The uniform grid represents the research area; each cell contains certain information.
(2) Time advances by discrete steps.
(3) System laws are given as a set of rules, according to which any cell can calculate its state at any time instant $t + 1$ based upon its state and the states of its closest neighbours at the time instant. It should be noted that these laws may have either a dynamic or a stochastic character; the latter allows random processes to be investigated.
(4) Also it is possible to take into account information about other previous time instants ($t - 1$, $t - 2$, etc.) which allows processes with memory to be simulated.

An important feature of cellular automata is the possibility of parallelizing calculations which sharply decreases the time of calculations. By means of numerical experiments, the cellular automata allow the dependence of the macrobehaviour of the whole ensemble of cells on the local microscopic laws that determine the evolution of each cell and its interaction with the closest neighbourhood to be studied.

The original solution of the present authors is the self-similar structure of cellular automata that allows the fractal nature of real materials to be modelled.

The goals of this article are as follows: to present the major structures and relations of cellular model of polycrystal and to test this model for its adequacy in describing the known effects and dependences; to illustrate this model while building the 'cloud of internal stresses' in a specific case; to show the evolution of this cloud

during its interaction with the 'thick yield surface'. Identification of the model, its application for studying of concrete polycrystals, and the investigation of the 'thick yield surface' structure and its interaction with material deformation mechanisms will be the subjects of future research.

§ 2. Model of the polycrystalline structure

According to present-day views, the deformable polycrystals have a multilevel hierarchical structure. There are four main scale levels that can be distinguished (Vladimirov and Romanov 1985):

(1) microscopic (atomic) with a characteristic size $l_{mic} = (1\text{-}30)a$, where a is the lattice constant;
(2) mesoscopic (dislocation substructures level) with a characteristic size $l_{sub} = 0.1\text{-}3\ \mu m$;
(3) structural (grain level) with a characteristic size $l_{str} = 20\text{-}200\ \mu m$;
(4) macroscopic with a characteristic size $l_{mac} > 10 l_{str}$.

Within mesoscopic and structural levels, the polycrystal has a fractal structure (Hornbogen 1986), the distinctive feature of which is the self-similarity on a changing view scale.

The actual polycrystal described above is modelled with a three-dimensional (3D) cellular structure. We assume that the RVE of polycrystal consists of the aggregate of interconnected units, namely cells; each of these can be either simple or complex. Simple cells simulate single crystals and do not contain any other cells. Complex cells, in turn, consist of simple and/or complex cells. As a component, a complex cell may contain cells similar to itself, which simulates the fractal nature of such structures (see figure 1 (*c*)).

In the present work, the complicated cells that have a cubic lattice structure are used. They consist of 27 ($3 \times 3 \times 3$) smaller cells (figure 2). In general, other spatial structures and other number of components are possible.

Note that the described units (cells) should not be considered in a literal sense as material cubes. According to the cellular automata approach (Toffoli and Margolus 1987), they are just objects that store certain information. In our case, these are the

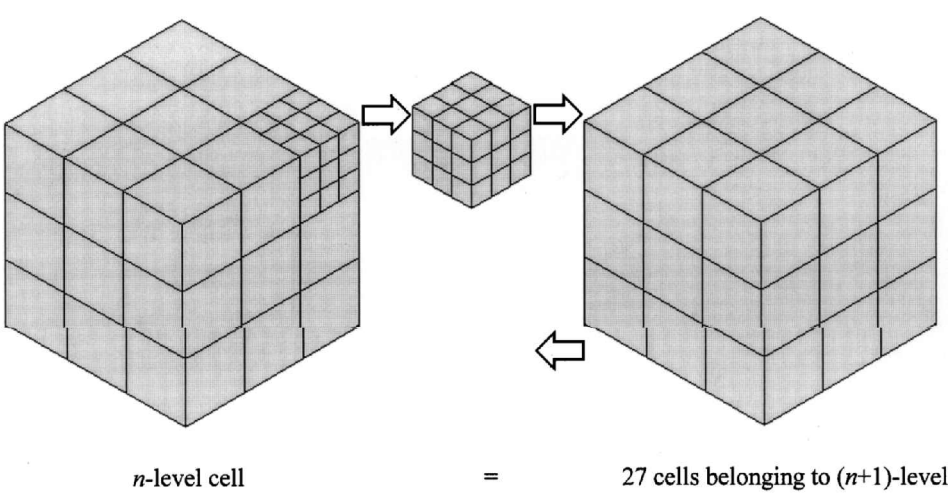

Figure 2. Model of the polycrystal structure.

parameters of stress–strained conditions (SSCs), which indicate the class of object, etc. (a detailed description is given below).

The above description defines a multilevel hierarchical structure. At zero level, there is just one cell (the material RVE), at the first level – 3^3 cells, at the second level – $(3^3 - p_1)3^3$, at the third level $[(3^3 - p_1)3^3 - p_2]3^3$, etc., where p_i is the number of simple cells on level *i*.

Each cell is denoted by triples of integers. Thus, the notation for a cell of the first level consists of only one triple (m, n, k), where *m, n, k* are integers varied from 1 to 3 (see figure 2). The second-level cells are denoted by two triples $(m_1, n_1, k_1)(m_2, n_2, k_2)$. The first specifies a parent first-level cell containing a given second-level cell, etc. To avoid repetition, not the full cell notation but just its level is indicated.

§ 3. Model of plastic deformation on polycrystals

The plastic deformation of a complex unit is carried out by joint strain and rotation of units contained in it. The inelastic deformation of a simple unit occurs by dislocation glide. According to Taylor (1938), the material flows through the crystalline lattice while the latter can rotate irreversibly. We do not consider elastic distortions and lattice curving.

The kinematics of plastic deformation of a cell are characterized by the velocity gradient $\mathbf{L}$ (Asaro 1983)

$$\mathbf{L} = \mathbf{D} + \boldsymbol{\Omega}, \tag{1}$$

where $\mathbf{D}$ is the symmetrical tensor of plastic extension velocities and $\boldsymbol{\Omega}$ is the anti-symmetrical tensor of rotation velocities.

Similarly to work (Asaro 1983), $\boldsymbol{\Omega}$ is decomposed into two components:

$$\boldsymbol{\Omega} = \boldsymbol{\Omega}^{\mathrm{p}} + \boldsymbol{\Omega}^{*}, \tag{2}$$

the first of which (indicated by a superscript p) is due only by plastic glide, and the second (indicated by an asterisk) arises because of rotation of the crystalline lattice.

For simple cells, according to Asaro (1983), we have

$$\mathbf{D} = \sum_{\alpha=1}^{k} \mathbf{P}^{(\alpha)} \cdot \dot{\gamma}^{(\alpha)}, \tag{3}$$

$$\boldsymbol{\Omega}^{\mathrm{p}} = \sum_{\alpha=1}^{k} \mathbf{W}^{(\alpha)} \cdot \dot{\gamma}^{(\alpha)}, \tag{4}$$

where

$$\mathbf{P}^{(\alpha)} = \tfrac{1}{2}(\mathbf{s}^{(\alpha)} \cdot \mathbf{m}^{(\alpha)} + \mathbf{m}^{(\alpha)} \cdot \mathbf{s}^{(\alpha)}), \tag{5}$$

$$\mathbf{W}^{(\alpha)} = \tfrac{1}{2}(\mathbf{s}^{(\alpha)} \cdot \mathbf{m}^{(\alpha)} - \mathbf{m}^{(\alpha)} \cdot \mathbf{s}^{(\alpha)}); \tag{6}$$

$\mathbf{m}^{(\alpha)}$ and $\mathbf{s}^{(\alpha)}$ are singular vectors that are normal to the sliding plane and to sliding direction respectively, in the aggregate defining active sliding system α; $\dot{\gamma}^{(\alpha)}$ is the crystallographic slip rate.

The magnitude of $\dot{\gamma}^{(\alpha)}$ is determined by the tangential stress τ^{α} acting in the appropriate sliding system (Asaro 1983) (see the detailed description below). The latter is calculated from the formula

$$\mathbf{t}^{(\alpha)} = \mathbf{m}^{(\alpha)} \cdot \mathbf{s}^{(\alpha)} : \Sigma, \tag{7}$$

where Σ is a stress tensor applied to simple unit.

The tensors $\mathbf{D}^n$ and $\Omega^{p,n}$ describing any complex n-level unit are determined by averaging:

$$\mathbf{D}^n = \frac{1}{27}\sum \mathbf{D}^{n+1}, \quad \Omega^{p,n} = \frac{1}{27}\sum \Omega^{p,n+1}, \tag{8}$$

where the summation is made on 27 component $(n+1)$-level units, which form a selected n-level unit. The relationships for $\Omega^{*,n}$ will be obtained below.

According to equations (4) and (8), in the general case, each $(n+1)$-level unit rotates as a whole in relation to its parent n-level unit. It activates the reaction from the power unit counteracting this rotation; this quantitative measure is the force moment connected with moment stresses. The force moment can be taken into account by the asymmetrical stress tensor Σ:

$$\Sigma = \boldsymbol{\sigma} + \mathbf{r}, \tag{9}$$

where $\boldsymbol{\sigma}$ and $\mathbf{r}$ are the symmetric and antisymmetric parts respectively of Σ.

The general theory of asymmetric elasticity was developed by Cosserat and Cosserat (1909). It was not appreciated during their lifetime but was redeveloped and extended by Truesdell and Toupin (1960). Simplified variants of the Cosserat–Cosserat medium theory have also been given by Mindlin and Tiersten (1962) and Koiter (1964). The main simplifying assumption of these studies is that the symmetrical part of the stress tensor is connected only with the symmetrical strain tensor. In the present work we also make this assumption.

The magnitude of the symmetrical part of stress tensor is determined using the self-consistent field approach. In order to calculate the stressed state of any unit belonging to $(n+1)$ level, the stressed state of the complex n-level parent unit is accepted as the average field of stresses. On the other hand, the gradient of the complex unit velocity is determined by averaging its components. Thereby, the correlation between the various levels of plastic deformation is simulated.

Corresponding to the above statement, we shall generalize the relationships of the self-consistent field theory for the symmetrical part of stress tensor (Berveiller and Zaoui 1979) taking into account the possibility rotation of the units:

$$\overset{\nabla}{\boldsymbol{\sigma}}{}^{n+1} - \overset{\nabla}{\boldsymbol{\sigma}}{}^{n} = \mathbf{M} : (\mathbf{D}^n - \mathbf{D}^{n+1}), \tag{10}$$

$$M_{jklm} = M\,\delta_{jl}\delta_{km}, \tag{11}$$

$M = 2a\mu(1-b)$ is the 'effective' elastic modulus, μ is the elastic shear modulus, $b = 2(4-5\nu)/15(1-\nu)$, ν is Poisson's ratio, and a is the 'plastic accommodation function' introduced by Berveiller and Zaoui (1979) in order to take into account the plastic accommodation of grain boundaries; a is varied from zero to one and is determined from the results of mechanical testing of polycrystals.

Equation (10) links the SSC properties of any complex n-level unit with those of the $(n+1)$-level units contained in it. In this relationship, ∇ designates the Jaumann derivative along the coordinate axis rotating together with the n-level units.

We now evaluate the magnitude of stresses and moments connected with the relative rotations of units. For this purpose we shall cut off an $(n+1)$-level unit from a n-level unit and extend it uniaxially along axes 2 (figure 3). Suppose that there was a rotation of the $(n+1)$-level unit by a small angle $\Delta\varphi_3^{n+1}$ in relation to the n-level unit. The latter initiates the moment opposite to the rotation. It is natural to assume as a first approximation that the magnitude of this moment is proportional to

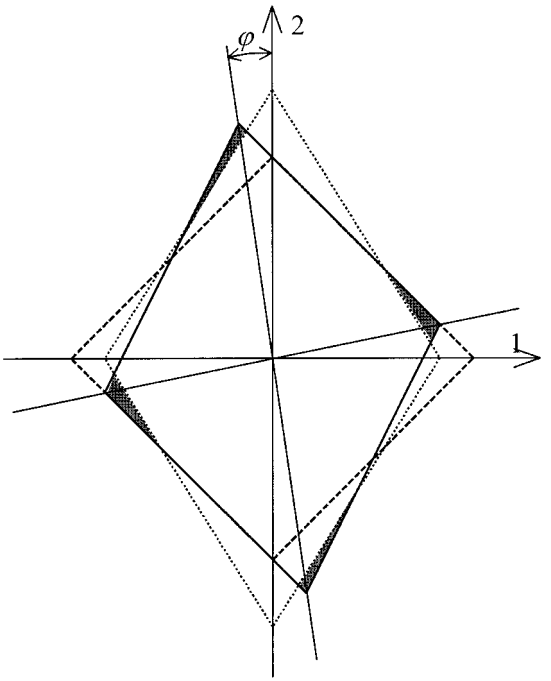

Figure 3. Small rotation of the $(n+1)$-level unit in relation to its parent n-level unit on uniaxial extension along axes 2: (———), $(n+1)$-level boundary after uniaxial extension; ('''''''), boundary of the 'hole' in the n-level element after uniaxial extension; (- - - - -), boundaries of the initial element and the hole before uniaxial extension.

$\Delta\varphi_3^{n+1}$. From dimensionality reasons,

$$\Delta\mu_3^{n+1} = -m(l^{n+1})^2 \Delta\varphi_3^{n+1}, \tag{12}$$

where $\Delta\mu_3$ is the moment component along axes 3, l^{n+1} is the characteristic linear size of $(n+1)$–level unit, and m is the material parameter in megapascal metres. The minus sign shows that the moment counteracts the rotation. As a vector,

$$\Delta\boldsymbol{\mu}^{n+1} = -m(l^{n+1})^2 \Delta\boldsymbol{\phi}^{n+1}. \tag{13}$$

On the other hand, it is possible to express the magnitude of $\Delta\mu_3$ through the asymmetric part of the stress tensor. From dimensionality reasons (with accuracy up to constant) we have

$$\Delta\mu_3^{n+1} = (l^{n+1})^3 \Delta r_{12}^{n+1}. \tag{14}$$

From equations (12) and (14) it follows that

$$\Delta r_{12}^{n+1} = -\frac{m}{l^{n+1}} \Delta\varphi_3^{n+1}. \tag{15}$$

Similar relationships can be obtained for Δ_{13}^{n+1} and Δ_{23}^{n+1}. Briefly, all these relationships can be written as follows:

$$\Delta r_{ij}^{n+1} = -\frac{m}{l^{n+1}} \varepsilon_{ijk} \Delta\varphi_k^{n+1}, \tag{16}$$

where ε_{ijk} is the Levi–Civita symbol.

Note that the Δr^{n+1} components, which are determined according to equation (16), represent this tensor within the frame rotating together with the $(n+1)$-level unit.

According to equation (2), the vector $\Delta\boldsymbol{\phi}^{n+1}$ can be decomposed on two components

$$\Delta\boldsymbol{\phi}^{n+1} = \Delta\boldsymbol{\phi}^{p,n+1} + \Delta\boldsymbol{\phi}^{*,n+1}, \tag{17}$$

the meanings of which correspond to $\boldsymbol{\Omega}^{p,n+1}$ and $\boldsymbol{\Omega}^{*,n+1}$. The component $\Delta\boldsymbol{\phi}^{p,n+1}$ initiates the elastic response of the environment $\Delta\boldsymbol{\mu}^{p,n+1}$, counteracting a rotation. $\Delta\boldsymbol{\mu}^{p,n+1}$ is evaluated from equation (13), where $\Delta\boldsymbol{\phi}^{p,n+1}$ is substituted for $\Delta\boldsymbol{\phi}^{n+1}$.

$$\Delta\boldsymbol{\mu}^{p,n+1} = -m(l^{n+1})^2\,\Delta\boldsymbol{\phi}^{p,n+1}. \tag{18}$$

The rotation $\Delta\boldsymbol{\phi}^{*,n+1}$ has the opposite sign and results in relaxation of the moment by the magnitude

$$\Delta\boldsymbol{\mu}^{*,n+1} = -m(l^{n+1})^2\,\Delta\boldsymbol{\phi}^{*,n+1}. \tag{19}$$

We now calculate each component of $\Delta\boldsymbol{\phi}^{n+1}$ separately. For this purpose we shall consider a complex *n*-level unit containing an $(n+1)$-level unit. The magnitude of $\Delta\boldsymbol{\phi}^{p,n+1}$ for the $(n+1)$-level unit is found from the formula

$$\Delta\varphi_i^{p,n+1} = \varepsilon_{ijk}(\Omega_{kj}^{p,n+1} - \Omega_{kj}^{p,n})\,\Delta t, \tag{20}$$

where Δt is the short time instant; $\boldsymbol{\Omega}^{p,n}$ is found according to equation (8) for complex units, except for the 0-level unit, and for simple units according to equation (4). For the 0-level unit we suppose that $\boldsymbol{\Omega}^{p,0} = \mathbf{0}$, that is we assume that all rotations of the structural elements and moment stresses are localized within the limits of material RVE.

The $\Delta\boldsymbol{\phi}^{*,n+1}$ components are determined by the following relationships:

$$\Delta\varphi_i^{*,n+1} = \begin{cases} 0, & \text{if } \kappa_i^{n+1} < \kappa_c, \\ -\Delta\varphi_i^{p,n+1}, & \text{if } \kappa_i^{n+1} \geqslant \kappa_c, \end{cases} \tag{21}$$

where $\kappa_i^{n+1} = |\mu_i^{n+1}|/(l^{n+1})^2$; κ_c is a material parameter with the units megapascal metres.

Equations (16), (19) and (21) show that the rotation of material units causing the relaxation of moments occur at a certain magnitude of the internal moment.

The tensor $\boldsymbol{\Omega}^{*,n+1}$ of velocities of these rotations is connected to $\Delta\boldsymbol{\phi}^{*,n+1}$ by

$$\Delta\varphi_i^{*,n+1} = \varepsilon_{ijk}(\Omega_{kj}^{*,n+1} - \Omega_{kj}^{*,n})\,\Delta t. \tag{22}$$

As we neglect the elastic distortions of the crystalline lattice, the tensor $\boldsymbol{\Omega}^{*,n+1}$ determines the modification of frame orientation of the $n+1$ unit in relation to its parent *n* unit.

Now we suppose that the appropriate Cartesian frames are displaced by the angles α, β, γ (Figure 4). For simplicity, we use the terms the 'upper system' for the *n*-level unit and the 'lower system' for the $(n+1)$-level unit. The transformation of coordinates of any vector $\mathbf{a}$ from the lower system to the upper system is determined by the matrix c_{ik}:

$$\bar{a_i} = \bar{c_{ik}} a_k, \tag{23}$$

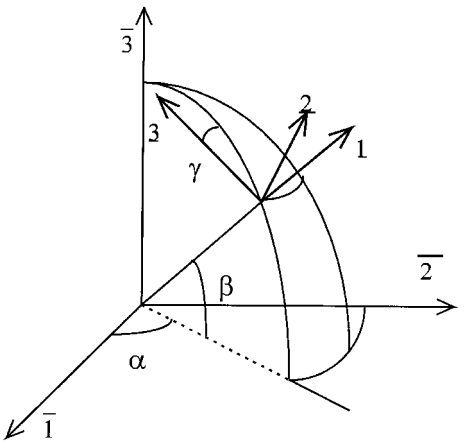

Figure 4. 'Upper' and 'lower' system interconnections.

where

$$
\begin{aligned}
c_{\bar{1}1} &= \cos\beta\cos\alpha,\\
c_{\bar{2}1} &= \cos\beta\sin\alpha,\\
c_{\bar{3}1} &= \sin\beta,\\
c_{\bar{1}2} &= -\cos\gamma\sin\alpha - \sin\gamma\cos\alpha\sin\beta,\\
c_{\bar{2}2} &= \cos\gamma\cos\alpha - \sin\gamma\sin\alpha\sin\beta,\\
c_{\bar{3}2} &= \sin\gamma\cos\beta,\\
c_{\bar{1}3} &= \sin\gamma\sin\alpha - \cos\gamma\sin\beta\cos\alpha,\\
c_{\bar{2}3} &= -\sin\gamma\cos\alpha - \cos\gamma\sin\beta\sin\alpha,\\
c_{\bar{3}3} &= \cos\gamma\cos\beta.
\end{aligned}
\tag{24}
$$

The index lines that are put above and below the values in figure 4 specify the upper and lower systems accordingly. It is easy to show that, as a result of unit rotation on a vector $\Delta\boldsymbol{\phi}^*$, the angles determining its orientation will be changed according to

$$
\begin{aligned}
\Delta\alpha &= \Delta\varphi^*_{\bar{3}},\\
\Delta\gamma &= \Delta\varphi^*_{\bar{3}}\sin\beta + (\Delta\varphi^*_{\bar{1}}\cos\alpha + \Delta\varphi^*_{\bar{2}}\sin\alpha)\cos\beta,\\
\Delta\beta &= \Delta\varphi^*_{\bar{1}}\sin\alpha - \Delta\varphi^*_{\bar{2}}\cos\alpha.
\end{aligned}
\tag{25}
$$

The relationships given in this paragraph allow a systematic computing process that simulates plastic deformation of polycrystal to be realized. To explain this process, we shall consider a cellular model unit state at an instant t and its modification at the time step Δt. As the model state we understand the stressed state properties of units.

Let us suppose that all these properties are known at t. At the next calculation step, the time increment Δt and the stress tensor symmetrical part increment $\Delta\sigma^0$ are

given at the upper level ($n = 0$). The modification of the model state happens in two stages. At the first stage, which we call 'movement downwards', the values of $\Delta\boldsymbol{\sigma}^n$, $\boldsymbol{\sigma}^n$, $\Delta\mathbf{r}^n$, $\mathbf{r}^n$, $\Delta\boldsymbol{\mu}^n$, $\boldsymbol{\mu}^n$ and $\Delta\varphi^{*,n}$ are determined. Here the kinematic characteristics $\mathbf{D}^n$, $\boldsymbol{\Omega}^{p,n}$, $\Delta\varphi^{*,n}$, α^n, β^n and γ^n of condition t are used. At the second stage, 'movement upwards', new values of the deformed state properties $\mathbf{D}^n$, $\boldsymbol{\Omega}^{p,n}$, α, β and γ are determined on the basis of the calculated stressed state parameters. The meanings of the terms 'movement downwards' and 'movement upwards' are as follows. At the first stage, the stressed state of units belonging to deeper scale levels is determined gradually; at the second stage, the deformed state properties of upper level units are determined by averaging over lower-layer units.

At $t = 0$ we suppose that $\mathbf{D}^n = 0$, $\boldsymbol{\Omega}^{p,n} = \mathbf{0}$.

The algorithm of the 'soft' loading simulation of polycrystals is stated above. By soft loading we mean a mode when the increments of the stress tensor $\Delta\boldsymbol{\sigma}^0$ are set at each step. The 'hard' loading mode is characterized by setting the increment of the full strain tensor $\Delta\mathbf{e}^0$ for the top-level unit ($n = 0$) at each time instant. In this case, $\Delta\boldsymbol{\sigma}^0$ is found from

$$\Delta\boldsymbol{\sigma}_0 = \mathbf{E} : (\Delta\mathbf{e}^0 - \mathbf{D}^0 \Delta t), \tag{26}$$

where $\mathbf{E}$ is the tensor of the polycrystalline elasticity modules.

With the help of equation (26), the simulation of 'hard' loading is reduced to the previous algorithm.

§ 4. Constitutive relationships for single crystals

Within the model framework offered, each simple unit that simulates a single crystal can have several sliding systems. They are set by the vector that is normal to the sliding plane and the vector, indicating the sliding direction in a simple unit frame. For each sliding system, the parameters of the constitutive relationships are specified.

The relationships connecting $\dot{\gamma}^\alpha$ with τ^α for various mechanisms, which control the movement of dislocations, have been given in a number of publications on plastic deformation physics.

In particular, according to Frost and Ashby (1982)

$$\dot{\gamma}^\alpha = \dot{\gamma}_0^\alpha \exp\left\{-\frac{\Delta F}{kT}\left[1 - \left(\frac{|\tau^\alpha|}{\tau_c^\alpha}\right)^p\right]^q\right\}\frac{\tau^\alpha}{\tau_c^\alpha}, \tag{27}$$

where ΔF is the energy of activation necessary to overcome obstacles in the absence of external stresses, τ_c^α is the critical tangential stress for system α, p and q are parameters dependent on the mechanism controlling dislocation glide ($0 \leqslant p \leqslant 1$; $1 \leqslant q \leqslant 2$), k is the Boltzman constant, t is the temperature and $\dot{\gamma}_0$ is the parameter describing system α.

Apart from equation (27), in the present work we have also taken advantage of the simple law used earlier by Asaro (1983):

$$\dot{\gamma}^\alpha = \dot{\chi}^\alpha \left(\frac{\tau^\alpha}{g^\alpha}\right)\left(\frac{|\tau^\alpha|}{g^\alpha}\right)^{1/\eta - 1}, \tag{28}$$

where $\dot{\chi}^\alpha$, g^α and η are parameters of system α. At $\eta \ll 1$ the last parameter corresponds to the critical tangential stress in equation (27), because an approximating $|\tau^\alpha|$ to $|g^\alpha|$ the velocity of a strain determined by equation (28) increases sharply.

The two laws mentioned above can be used for both velocity-sensitive and velocity-insensitive materials. In the latter case, the parameters of equations (27) and (28) should be such that the derivative $\dot{\gamma}^{\alpha}$ on τ^{α} at $|\tau^{\alpha}| > \tau_c^{\alpha}$ ($|\tau^{\alpha}| > g^{\alpha}$) is large enough (see the more detailed description in the section on the analysis of computer experiments).

Deformational hardening of single crystals corresponds to the dependences of τ_c^{α} and g^{α} on the magnitude of sliding strain. The various models of self-hardening and latent hardening of sliding systems are comprehensively analysed by Asaro (1983). In the present work, we used the following simplified model of deformational hardening:

$$\tau_c^{\alpha} = \tau_{c0}^{\alpha} \left(1 + C_1\gamma^{\alpha} + C_2 \sum_{\beta \neq \alpha} \gamma^{\beta}\right), \tag{29}$$

where $\gamma^{\alpha} = \int_0^t |\dot{\gamma}^{\alpha}| \, dt$, and C_1 and C_2 are constants.

The second and third terms in equation (29) characterize the self-hardening of system α and its latent hardening that is caused by other sliding systems.

§ 5. Comparison of the cellular model with the classical self-consistent scheme

There are three major differences between the cellular model and the classical self-consistent scheme:

(1) The stressed condition of elements at instant t is determined by their strained condition at instant $t - 1$, instead of instant t, as in the classical self-consistent scheme.
(2) The response of the closest surrounding is taken into account while determining the stressed condition of elements.
(3) The response of the environment connected with the rotations of elements is taken into account.

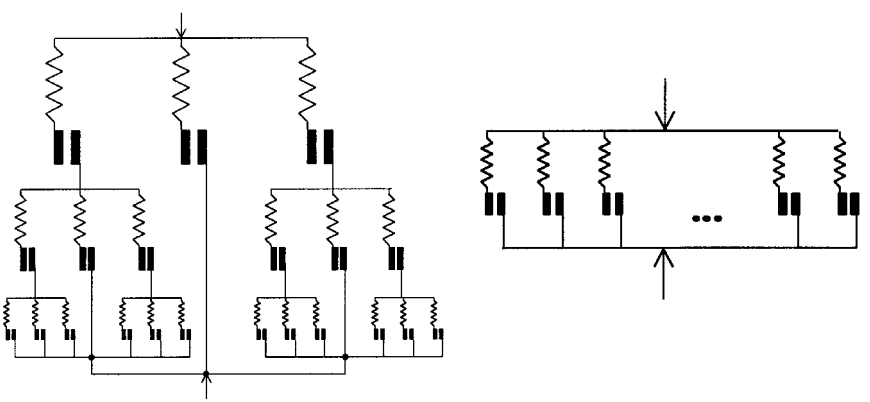

(*a*) (*b*)

Figure 5. Simple rheological models illustrating the differences in the determination of the environment response for (*a*) the cellular model and (*b*) the classical self consistent scheme.

The indicated differences allow the following:

(*a*) use of the cellular model for investigation of aggregates with inhomogeneous and fractal structures;
(*b*) incorporation of the local character of interaction of grains (short-range interaction);
(*c*) consideration of various material hardening laws, which can be not only linear, as in the work of Berveiller and Zaoui (1979);
(*d*) use of different material parameters (such as the accommodation function and the characteristic linear dimension) at different scale levels.

Simple rheological models illustrating the differences in the determination of the environment response for the cellular model and the classical self-consistent scheme are shown in figure 5.

§ 6. Computer experiments with the cellular model of polycrystal

On the basis of the model of polycrystal deformation described above, we designed some personal computer software. The structure of the circumscribed model meets the modern object-oriented computer programming approach. The model unit is described as an easily readable programming object that can be modified and improved in use. A number of such objects corresponding to various material structures have been developed. Any material can be simulated by the appropriate combination of base objects stored in a supplemented object database.

The random access memory (RAM) volume is critical to execute the application. For instance, to simulate a four-level system of fcc material (12 sliding systems are allowed in cells of the lower fourth level) about 6 Mbytes of RAM are needed. The original software had been tested on Pentium 233 MMX with 32 Mbytes of RAM. Application allows the behaviour of any unit to be monitored during the deformation of the whole aggregate; stress–strain curves and plasticity surfaces for a specific inelastic strain value to be obtained and the creation of textures, etc., to be predicted.

The major task of computer experiments was to investigate and analyse the properties and convergence of the computing process, to test the cellular model for an adequate description of already-known effects and regularities, and to reveal the dependence of the deformation process on model parameters. The following tasks will be the subject of future research: identification of the model parameters; its quantitative comparison with the full-scale experiment; use of model for the research of real polycrystal plastic flow regularities.

As has already been mentioned above, the software based on cellular model allows one 'to enter' (navigate through) any unit instantly during the calculations and to monitor the modification of its SSC properties.

Using these features, in particular, it was determined that the constitutive relationships (27) and (28) maintain the tangential stress τ^α at the level $\tau_c^\alpha(g^\alpha)$. Relative deviations in these magnitudes do not exceed 5–7%. The reason for this is that at $|\tau^\alpha| > \tau_c^\alpha(|\tau^\alpha| > g^\alpha)$ the strain γ^α increases sharply as τ^α increases, which entails the response of the environment reducing τ^α. Because of discretization of the calculation process, a decrease in $|\tau^\alpha|$ to a level below $\tau_c^\alpha(|\tau^\alpha| > g^\alpha)$ is possible, which results in a practical stoppage of the strain in system α. Then, continuing loading in this direction, the magnitude of $|\tau^\alpha|$ increases and, after several time instants, the system begins to work again. Systems with the indicated behaviour were considered to be active. Systems which have $|\tau^\alpha| < \tau_c^\alpha(|\tau^\alpha| < g^\alpha)$ during the final time instant were

called passive. The number of active sliding systems on each loading step is determined using the magnitude of the accumulated strain and the following model parameters: the number of allowed sliding systems; the 'effective' elastic modulus M; the parameters m, κ_c, C_1 and C_2. As M, m, κ_c and C_1 increase, there is a tendency for the number of active systems to increase. The latter is caused by the decreased ability of units to be accommodated with the help of acting sliding systems, and that is why the unit is compelled to include new units. Numerical examples are given below.

In the case when adjacent units are deformed almost uniformly, the environment cannot stabilize the magnitude of tangential stresses, and the failure of the computing process during the soft loading mode is very probable because of the extremely high value of strain increment. This corresponds to the ideal plasticity case.

The major critical point for any discrete computing process is the influence of the argument increment (calculation step) on the outcome of the experiment. A reasonable answer to the question about a proper step requires additional theoretical research and is not considered in the present article. Practically, we have always managed to find such small increments of stresses (in the soft loading mode) or strains (in the hard loading mode) for which decreases by a factor of two or more almost had no effect on the outcome of calculation. It appeared that the calculation of one loading program up to strains of the order of 0.2 using the computer configuration indicated above takes about 10–15 min in an interactive mode.

As an example, we shall describe the outcome of experiments on the simulation of the multistage deformation of an iron polycrystal. The following values of the model parameters were used in the calculations: $\Delta F = 6 \times 10^{-19}$ J; $\tau_c = 100$ MPa; $\dot{\gamma}_0 = 10^{-5}\,s^{-1}$; $\mu = 80$ GPa (Frost and Ashby 1982); $T = 300$ K; characteristic size of units $l = 5 \times 10^{-7}$ m (in trial calculations the sizes are identical for all units); $m = 5 \times 10^{-5}$ MPa m. α, β and γ are distributed gradually within the following ranges: $\alpha \in [0, 2\pi]$; $\beta \in [-\pi/2, \pi/2]$; $\gamma \in [0, 2\pi]$. The value of $2\mu(1-b)$, which is present in the relationship for the effective elastic modulus, was 100 GPa. The various conditions for the experiment are given in table 1.

In figures 6 and 7, the results of computer experiments on the uniaxial extension of a polycrystal are shown. The dependences on the effective elastic modulus M (or 'plastic accommodation function' a) and the number of allowed sliding systems in simple units are given. The simulation where a large part of sliding systems is blocked was carried out separately.

Table 1. Conditions for the numerical experiments.

Experiment	Plastic accommodation function a	M (GPa)	Number of allowed sliding systems	κ_c (10^{-5} MPa m)
1	1	100	12†	10
2	0.5	50	12†	10
3	0.25	25	12†	10
4	1	100	4‡	10
5	0.5	50	4‡	10
6	0.25	25	4‡	10
7	0.5	50	12†	10
8	1	100	12†	1

† $(111)\langle 1\bar{1}0\rangle$.
‡ $(111)[110]$, $(\bar{1}11)[01\bar{1}]$, $(1\bar{1}1)[011]$, $(\bar{1}\bar{1}1)[011]$.

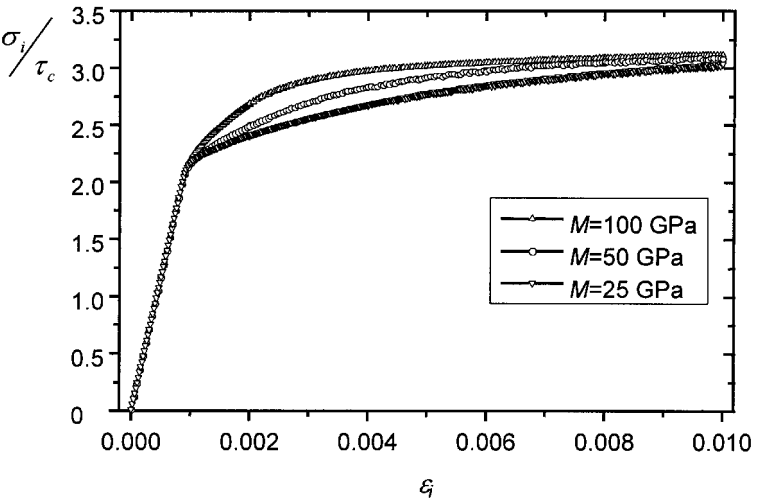

Figure 6. Influence of 'effective' elastic modulus M on the hardening curve for fcc material (table 1, experiments 1–3).

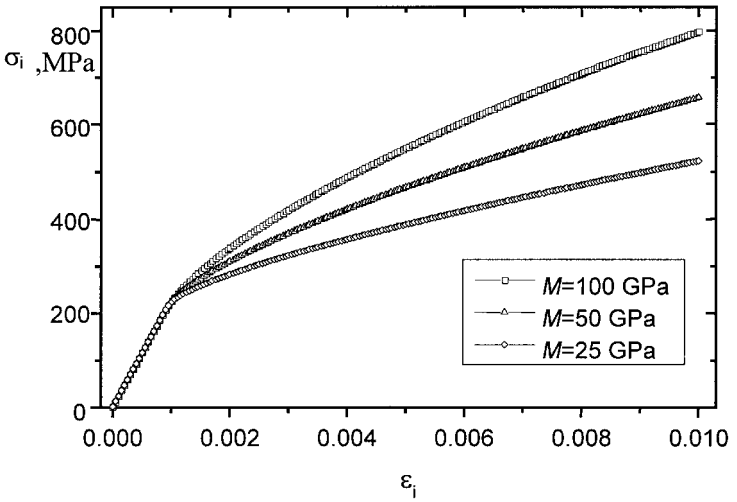

Figure 7. Influence of the 'effective' elastic modulus M on the hardening curve for the material with four allowed sliding systems (table 1, experiments 4–6).

The abscissae for these and the following figures indicate the magnitude of the full strain calculated using the equation

$$\varepsilon_i = \frac{2^{1/2}}{3} \sum [(\Delta e_{xx} - \Delta e_{yy})^2 + (\Delta e_{yy} - \Delta e_{zz})^2 + (\Delta e_{zz} - \Delta e_{xx})^2 + 6(\Delta e_{xy}^2 + \Delta e_{yz}^2 + \Delta e_{zx}^2)]^{1/2}, \quad (30)$$

where the summation is over all steps of deformation preceding the present moment of time and Δe_{ij} are the increments of full strains of the 0-level unit.

First, we should mention that the calculated magnitude of σ/τ_c (figure 6) corresponds to the value of 3.06 for this parameter given by Taylor (1938) and to the value of 3.1 given by Bishop and Hill (1951).

As expected, the decrease in M results in softening of the elastic response of the environment which corresponds to an increase in the efficiency of grain-boundary accommodation. This lowers the stress–strain curves.

Note that the decrease in the number of allowed sliding systems to four results in a sharp increase in the deformational hardening intensity of a polycrystal.

During the numerical experiments it was established that in the case of 12 possible sliding systems the number of active systems changed from two to four in different units, and in the case of four possible systems from three to four.

Figure 8 shows the influence of rotations on the shape of stress–strain curves. This draws attention to the fact that the linear part of these curves occurs in the

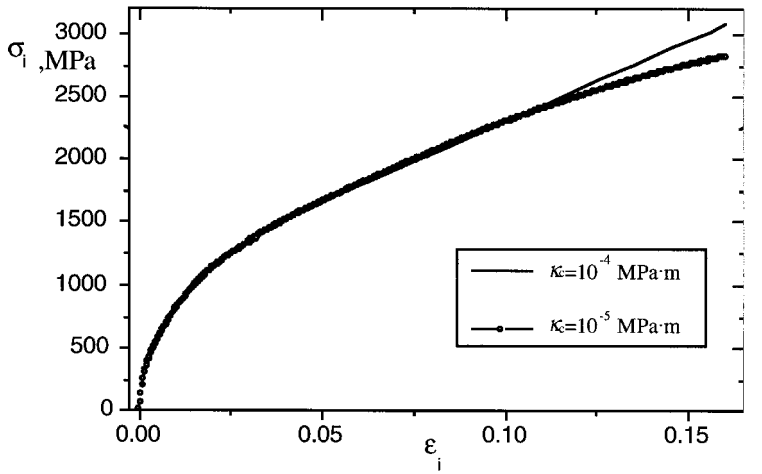

Figure 8. Influence of the rotations on the hardening curve for the material with four allowed sliding systems (table 1, experiment 7).

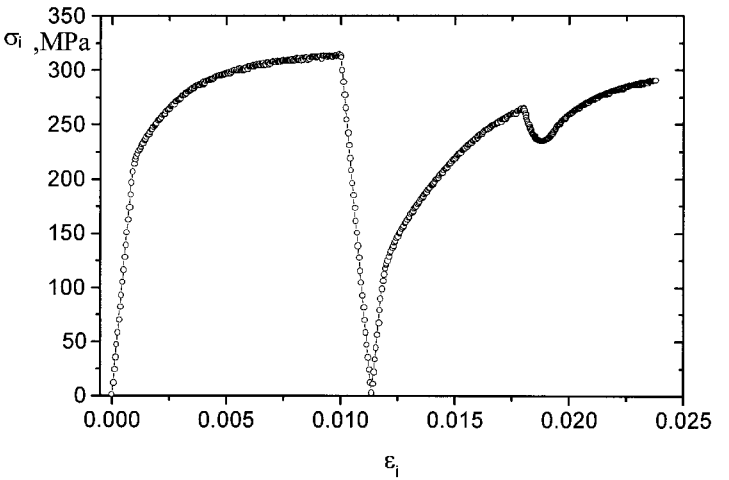

Figure 9. Non-monotonic deformation of fcc material (table 1, experiment 8).

Table 2. Program of complex deformation.

Step N	e_{xx}	e_{yy}	e_{zz}	e_{xy}	e_{yz}	e_{zx}
1	0	0	0	0	0	0
2	− 0.005	− 0.005	0.01	0	0	0
3	0	0	0	0	0	0
4	0	0	0	0.005	0	0

absence of rotations. The initiation of rotations results in the additional relaxation of internal stresses and parabolizes curves. These results correspond to the data from known experiments.

Figure 9 shows the hardening curve that was obtained for a polycrystal by the deformation program given in table 2.

In table 2, e_{ij} are the components of the full strain tensor of the material RVE (0-level cell). The following is worth noting: on unloading and loading in the opposite directions (step 3) the Bauschinger effect is exhibited. On glide deformation of solid, the temporary unloading of material happens at step 4; then the hardening curve disappears on prolonging the previous step curve. Here the known effect of the uniform hardening curve is exhibited.

§ 7. Polycrystal 'thick yield surface' and its structure

We now construct the yield surface of a polycrystal in a classical way with the help of the designed cellular model. Figure 10 (*a*) shows the results of calculations for experiment 1 (table 1); figure 10 (*b*) correspond to the same calculation conditions except that there is artificial texture for this material ($\alpha = \beta = \gamma = 0$ for all units); here the allowed residual strain is 10^{-3}. Figure 10 (*a*) approaches the van Mises ellipse; figure 10 (*b*) is very close to the Tresca hexagon.

The trace of the yield surface calculated at a very small residual strain tolerance (10^{-5}) is shown in figure 10 (*c*). Calculation results correspond well to the conclusions of Lipinski *et al.* (1990) who showed that the yield surface of a polycrystal is similar to the Tresca prism at the very small residual strain tolerance.

We shall now expand ideas about the yield surface. For this purpose, we shall map the yield surfaces of separate elements in the stress space as if they were not connected to each other. Obviously, the yield surface of each sliding system will be mapped by a pair of parallel planes, determined by the equation

$$|\mathbf{m}^{(\alpha)} \cdot \mathbf{s}^{(\alpha)} : \Sigma| = \tau_c^{(\alpha)}. \tag{31}$$

The point corresponding to the stressed state of this system can be either between the indicated planes (in this case system is not active) or on them (in this case system is active).

The conjunction of the yield planes of all sliding systems of simple units will eventually form the geometric object that we shall call the 'thick yield surface' of this unit. The quotation marks indicate that this term is used not in the classical way. The classical variant would be a yield surface representing the boundary of the intersection of elastic areas for all sliding systems of the considered unit (Koiter 1953).

The 'thick yield surface' of the *n*-level complex unit is a geometric object formed by the aggregation 'thick yield surfaces' of all $(n+1)$-level units contained in it. As a result of this construction in stress space, the self-similar geometric object is

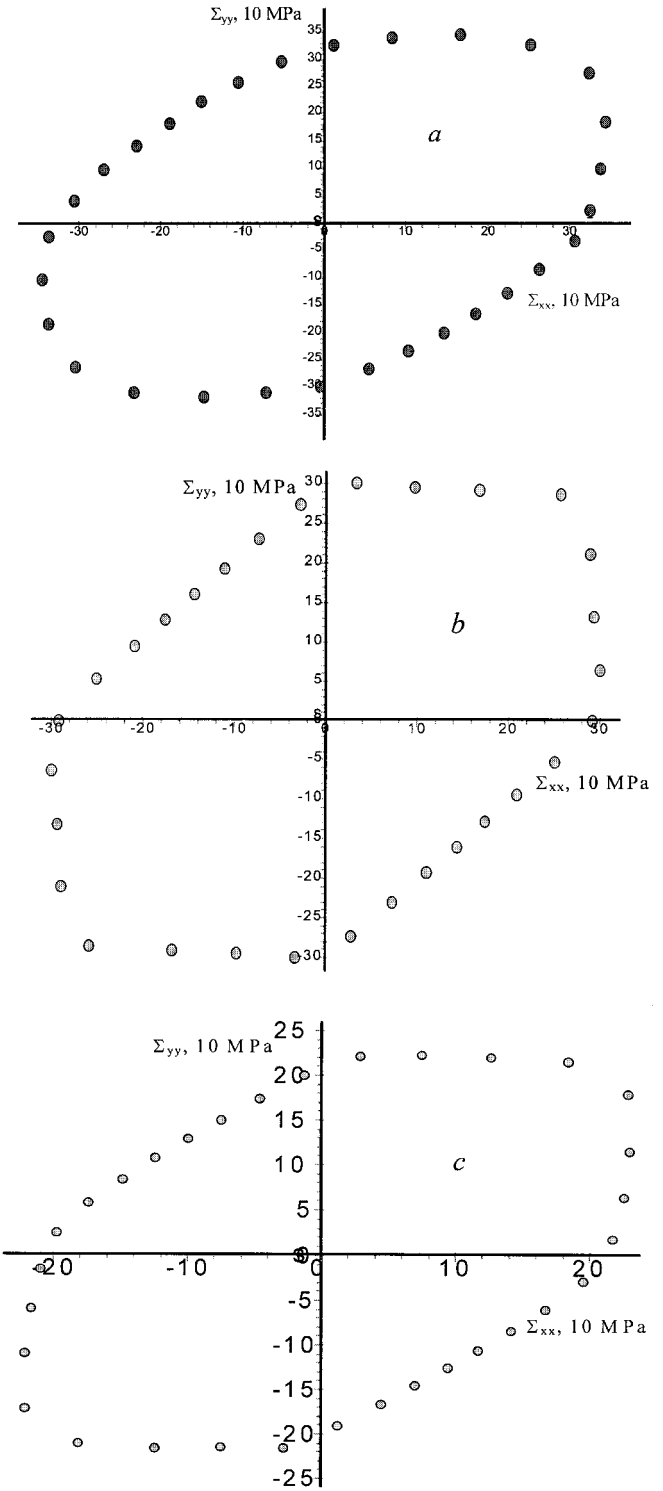

Figure 10. Calculated yield surface contours: (*a*) without texture; (*b*) textured material; (*c*) without texture at the very small residual strain tolerance (10^{-5}).

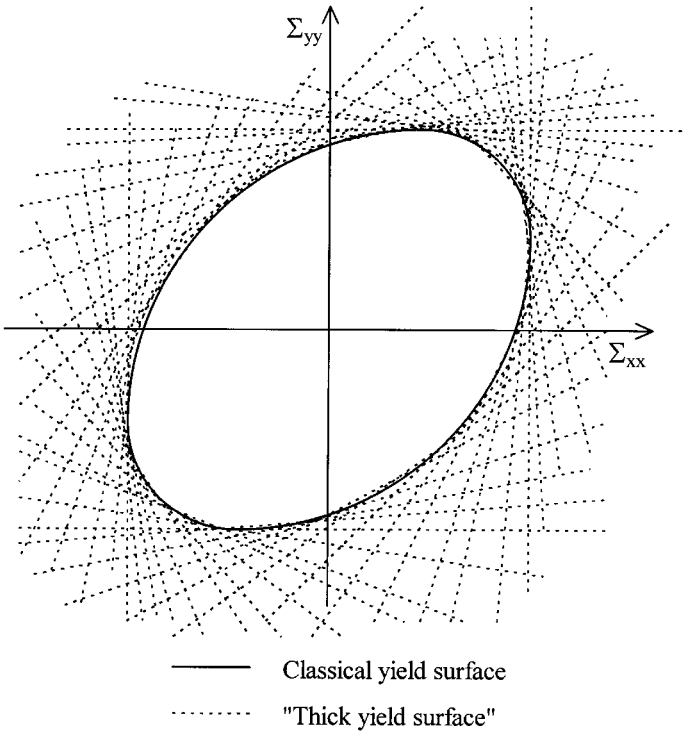

Figure 11. Difference between the classical yield surface and the thick yield surface.

obtained. We shall call it the 'thick yield surface' of a polycrystal. In the present work we propose a hypothesis that this object is of a fractal nature. Figure 11 shows the difference between the classical yield surface and the 'thick yield surface'.

Different from the classical yield surface, the 'thick yield surface' has an internal structure. The point mapping the stressed state of the material representative volume can penetrate inside this 'thick surface'. Here it can 'split', forming the set of points that map the stressed states of the first-level units. Each one of them can reside only within the limits of its unit 'thick yield surface', inside which this point, in turn, is 'split' into the points corresponding to the stressed states of the second-level units, etc. Finally, the stressed state of the representative volume of a polycrystal is mapped by a set of points N, which reside on yield planes of the corresponding sliding systems of the lowest-level units.

Obviously, the diameter of N is a quantitative measure of internal microstresses in the material. In figure 12 the evolution of N under the loading of the same material in different directions within the Σ_{xx}-Σ_{yy} plane is shown (the stressed states of units are given in 0-level unit coordinates). The calculation is carried out using the cellular model of a polycrystal under the conditions indicated above. The depth of a penetration inside the 'thick yield surface' corresponds to a residual strain magnitude of 0.01.

Figure 12 shows that each penetration of the set N in the 'thick yield surface' results in distortion of this set. The beginning of plastic flow of material is connected to the first signs of this distortion.

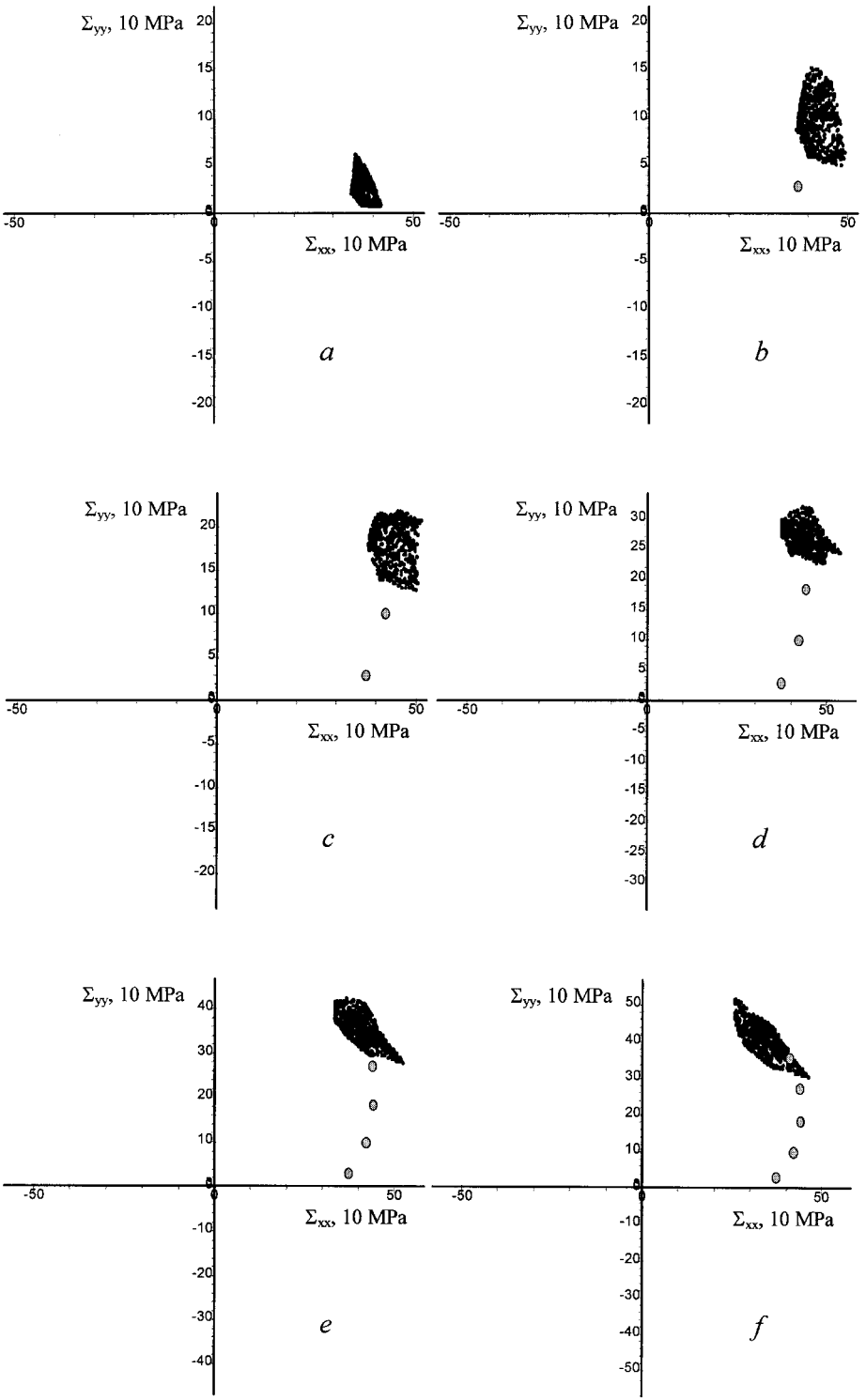

Figure 12. Evolution of N during the consequential penetration inside the 'thick yield surface'.

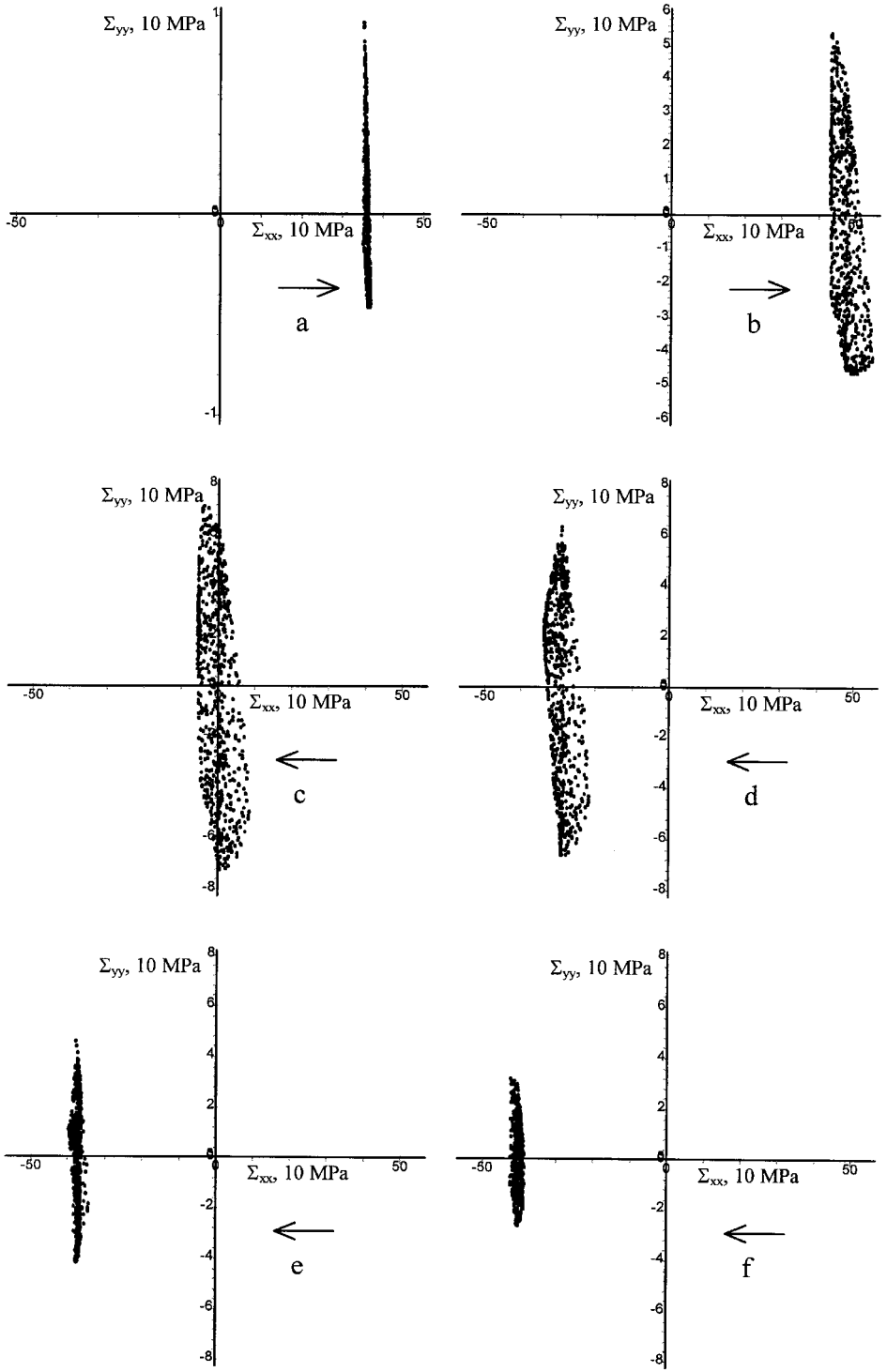

Figure 13. Evolution of N on complex two-stage loading: (*a*) initiation of splitting on direct loading; (*b*) N at the end of direct loading; (*c*) N after unloading; (*d*)–(*f*) distortion of N on opposite sign loading.

Figure 13 shows the evolution of N at the complex two-stage loading going in opposite directions. It is clearly seen that the set N starts to distort at the smaller outer stresses during opposite sign loading, compared with the initial loading, which reveals the Bauschinger effect.

While the magnitude of the penetration depth increases, the diameter of N increases as each of the mapping points can move only along the yield plane, which corresponds to the increase in internal stresses.

The latter reaches a maximum size and stops increasing at a certain value of the increasing strain. This means that at the rather deep penetration inside the 'thick yield surface' the yield planes should rotate or fractionate, stretching very considerably the set N. Obviously, the first stated effect corresponds to the rotation of units, and the second effect to the partition of simple units, producing parts rotated from one another (the fragmentation of grains). At the same time, a recess forms on the internal boundary of the 'thick yield surface'.

The classical yield surface determines the increment of plastic deformation at each loading stage (Hill 1950) by means of the associated flow law. It is easy to see that the 'thick yield surface' proposed by us has similar properties. The difference is that in this case the macroscopic vector of the plastic deformation increment of the representative volume is obtained by summation of the vectors of the microstrain increment of separate elements, which follows from equation (8). The increment of plastic deformations, which is stipulated by a sliding system, is determined by the vector that is orthogonal to the appropriate yield plane. The latter follows from equations (3), (5) and (31).

The velocity of the plastic deformation growth of a polycrystal depends on the structure of the 'thick yield surface' area, occupied by a set N, and on the direction of the vector of the macrostress increment defining the evolution of N. In this connection, even though the magnitude of movement into the 'thick yield surface' may be identical in specific cases, there may be different increments of plastic deformation in different parts of this surface and along the different directions of movement inside it. Here, ideal plasticity (plasticity without hardening) corresponds to some limiting formations in a 'thick yield surface'. To reach those, there should be indefinitely large residual strain.

§ 8. Conclusions

To summarize all that has been stated about the 'thick yield surface', it is possible to conclude that, for a number of reasons, it is an interesting object, especially when considered together with the 'cloud of internal stresses'. This object should not be reduced just to a new label. Several reasons for this are given below.

(1) The 'thick yield surface' allows one to distinguish between the hardening mechanisms connected with internal stresses and those connected with modifications in material structure. The former are revealed as modifications of the 'cloud of internal stresses' and have no effect on 'thick yield surface'; the latter change this surface.
(2) The 'thick yield surface' allows one to give a new geometric image to effects caused by internal stresses and by disproportionate loading and unloading. For example, the Bauschinger effect is explained not as a migration of the whole yield surface but rather as an extension of the 'cloud of internal stresses'. Plastic flow during the neutral additional loading (e.g. the

experiments of Nahdi and Rowley 1954) cannot be connected with the formation of the angular point on a smooth yield surface. Here, the centre of the 'cloud of internal stresses' (the point mapping the stressed state of RVE as whole) is moving inside the body of the 'thick yield surface'.

(3) Numerical experiments show that the size and the form of the 'cloud of internal stresses' depend on the trajectory and the length of path followed by the centre of this cloud along the trajectory of its movement inside the 'thick yield surface'. In turn, the geometry of the 'cloud of internal stresses' and local structure of the 'thick yield surface' determine the velocity of RVE deformation. All this encourages us to think that the geometric properties of the proposed objects can be used as parameters in the constitutive relationships for RVE.

The concept of the 'thick yield surface' allows one to obtain the additional correlation between the micromechanical models of polycrystals and the phenomenological theory of plasticity. Evidently, the 'thick yield surface' is of a fractal nature. The structure of this 'surface' as well as the other properties of a deformable polycrystal can be investigated with the help of the cellular model developed.

References

Asaro R. J., 1983, *J. appl. Mech.,* **50**, 921.

Barrenblatt, G. I., 1979, *Similarity, Selfsimilarity and Intermediate Asymptotics* (New York: Plenum).

Batdorf, S. B., and Budiansky, B., 1949, *National Advisory Committee for Aeronautics (NACA) Technical Note 1871.*

Berveiller, M., and Zaoul, A., 1979, *J. Mech. Phys. Solids,* **26**, 325.

Budiansky, B., and Wu, T. T., 1962, *Proceedings of the Fourth US National Congress on Applied Mechanics,* edited by R. M. Rosenberg (New York: American Society of Mechanical Engineering), p. 1175.

Bishop, J. F. W., and Hill, R., 1951, *Phil. Mag.,* **42**, 1298.

Cosserat, E., and Cosserat, F., 1909, *Theorie des Corps Deformables* (Paris: Hermann).

De Gebbes, P. G., 1979, *Scaling Concepts in Polymer Physics* (Ithaca, New York: Cornell University Press).

Eshelby, J. D., 1957, *Proc. R. Soc.* A **241**, 398.

Frost, H. J., and Ashby, M. F., 1982, *Deformation—Mechanisms, Maps* (Oxford: Pergamon).

Hill, R., 1950, *Mathematical Theory of Plasticity* (Oxford University Press), chapter 3; 1965, *J. Mech. Phys. Solids,* **13**, 89; 1972, *Proc. R. Soc.* A, **325**, 131.

Hornbogen, E., 1986, *Pract. Metall.,* **23**, 258.

Hutchinson, J. W., 1964, *J. Mech. Phys. Solids.,* **12**, 11.

Koiter, W. T., 1953, *Q. appl. Math.,* **11**, 350; 1964, *Proc. Koninklijke Nederlanse Akademie van Wetenschappen,* B, **67**, 17.

Kröner, E., 1961, *Acta metall.,* **9**, 155.

Lipinski, P., Krier, J., and Berveiller, M., 1990, *Rev. Phys. Appl.,* **25**, 361.

Mandelbrot, B., 1983, *The Fractal Geometry of Nature* (New York: W. H. Freeman).

Mindlin, R. D., and Tiersten, H. F., 1962, *Arch. Rational Mech. Anal.,* **11**, 415.

Nahdi, P. M., Rowley, J. C., 1954, *J. Mech. Phys. Solids,* **3**, 63.

Preston, K., and Duff, M., 1994, *Modern Cellular Automata, Theory and Applications* (New York: Plenum).

Rice, J. R., 1971, *J. Mech. Phys. Solids,* **19**, 433.

Shen, Y.-L., Finot, M., Needleman, A., and Suresh, S., 1994, *Acta metall. mater.,* **42**, 77.

Taylor, G. I., 1938, *J. Inst. Metals,* **62**, 307.

Toffoli, T., and Margolus, N., 1987, *Cellular Automata Machines* (Cambridge, Masssachussetts Institute of Technology).

Truesdell, C. A., and Toupin, R. A., 1960, *The Classical Field Theories, Encylopenia of Physics,* Vol. III/1 (Berlin: Springer).

Vladimirov, V. I., and Romanov, A. E., 1985, *Disclinations in Crystals* (Leningrad: Nauka).